Available online at www.sciencedirect.com
ScienceDirect
Journal of Computational Physics 218 (2006) 654–676
JOURNAL OF COMPUTATIONAL PHYSICS
www.elsevier.com/locate/jcp

A stochastic variational multiscale method for diffusion in heterogeneous random media

Badrinarayanan Velamur Asokan, Nicholas Zabaras *

Materials Process Design and Control Laboratory, Sibley School of Mechanical and Aerospace Engineering, 188 Frank H.T. Rhodes Hall, Cornell University, Ithaca, NY 14853-3801, USA

Received 26 October 2005; received in revised form 24 February 2006; accepted 27 February 2006
Available online 19 April 2006

Abstract

A stochastic variational multiscale method with explicit subgrid modelling is provided for numerical solution of stochastic elliptic equations that arise while modelling diffusion in heterogeneous random media. The exact solution of the governing equations is split into two components: a coarse-scale solution that can be captured on a coarse mesh and a subgrid solution. A localized computational model for the subgrid solution is derived for a generalized trapezoidal time integration rule for the coarse-scale solution. The coarse-scale solution is then obtained by solving a modified coarse formulation that takes into account the subgrid model. The generalized polynomial chaos method combined with the finite element technique is used for the solution of equations resulting from the coarse formulation and subgrid models. Finally, various numerical examples are considered for evaluating the method.

Keywords: Variational multiscale; Multiscale finite element; Operator upscaling; Stochastic diffusion; Subgrid modelling; Generalized polynomial chaos

1. Introduction

In this paper, we address a variational multiscale (operator upscaling) framework for numerical simulation of transient diffusion in a random medium whose diffusion coefficient is characterized by the presence of features at multiple length scales. The potential applications for the problem include heat transfer in composites [1,2] and flow in porous media [3], wherein, spatial variation in material properties requires a statistical description owing to gappy data and assumptions in constitutive models. Fully-resolved transient computations require spatial and temporal discretizations that can resolve the smallest length scales in the material data (here, the diffusion coefficient) and time scales in the solution, respectively. However, in practice, a coarse-scale description of the solution is deemed adequate. It is thus desirable to develop computational

* Corresponding author. Tel.: +1 607 255 9104; Fax: +1 607 255 1222.
E-mail address: zabaras@cornell.edu (N. Zabaras).
URL: http://mpdc.mae.cornell.edu (N. Zabaras).

0021-9991/$ - see front matter
doi:10.1016/j.jcp.2006.02.026

techniques that "solve for a coarse-scale solution by defining an appropriate coarse-scale problem that captures the effect of the fine-scales" [4]. This forms the backbone of most upscaling methods (see [5] for a comprehensive review).

Current research on upscaling techniques (more specifically, multiscale methods) aims at the derivation of a coarse-scale formulation that has the following characteristics: (i) it contains adequate fine-scale information, i.e. the fine-scale solution can be reconstructed from the coarse solution and subgrid results, (ii) the computation cost for the coarse-scale problem should scale sub-linearly with respect to the fully-resolved computation, and (iii) it should avoid assumptions of special problem structures like periodicity and scale separation. However, when these structures are present, we should be able to exploit them for increasing computation speed.

The most popular techniques developed for upscaling in deterministic context fall under the category of multiscale methods viz. the variational multiscale *VMS* method (also known as operator upscaling) [6–8], the heterogenous multiscale method [9,10], and the multiscale finite element method [11–13]. These methods typically involve introduction of multiscale basis functions at the coarse-scale. These multiscale basis functions include information about the fine-scale heterogeneities in the problem. Further related techniques involve the generalized finite element method [14] and the residual-free bubbles [15].

Parallel to the above developments in deterministic upscaling techniques, there have been considerable advances in computationally efficient stochastic analysis approaches. Traditionally, stochastic analysis techniques for partial differential equations (PDEs) involve Monte-Carlo sampling [16], perturbation analysis [17] and Neumann expansions [18]. However, these methods are limited either by the prohibitive computation cost, inability to handle large fluctuations and nonlinearity and/or complexity involved in derivation of these techniques (e.g. deriving perturbation methods for analyzing higher-order solution statistics becomes increasingly complex). These shortcomings are alleviated by using the generalized polynomial chaos expansion (GPCE) approach [19], a technique for representing stochastic fields with finite variance using Wiener–Askey hypergeometric polynomials [20,21]. The GPCE is a significant advancement on the spectral stochastic method [22] that uses Hermite polynomials for representing Gaussian and allied stochastic processes (e.g. log-normal process as an exponential of a Gaussian process). The GPCE approach has been used successfully in the context of fluid-flow [23,24], fluid-structure interaction [25] and natural convection [24]. A survey of numerical challenges in the implementation of the GPCE approach for the solution of stochastic PDEs is provided in [26].

Using deterministic upscaling techniques for statistical analysis of the solution typically involves the use of computationally expensive Monte-Carlo methods. Recently, there has been a considerable interest in stochastic homogenization, upscaling methods [27,28]. These methods however employ restrictive assumptions on the problem structure viz. periodicity and scale separation. However, considering the advances in deterministic upscaling methods and stochastic analysis approaches, it is time to address direct incorporation of the inherent randomness in material data and the effect of modelling assumptions in the design of upscaling methods. In this paper, we combine the variational multiscale VMS method [29,30], the multiscale finite element method and deterministic operator upscaling technique [1,3,4,6,11] and the GPCE/polynomial chaos approach [19,22] to derive a variationally consistent upscaling technique for the stochastic transient diffusion equation. The authors emphasize that though all of the above techniques are not a part of their original work, this paper introduces a framework to combine these techniques to derive a stochastic upscaling technique. Also, the paper addresses operator upscaling in the context of a transient multiscale diffusion equation, which to the best of the authors' knowledge is a novel contribution. Since randomness is effectively seen as an additional dimension in the problem [31], our method essentially performs upscaling for a class of problems corresponding to various realizations of the random material data (here, the diffusion coefficient).

The choice of VMS as the upscaling method and GPCE as the stochastic analysis method is motivated by a number of reasons. VMS and operator upscaling methods have emerged in recent years as computational paradigms for development of multiscale analysis [6,29]. The VMS approach essentially involves splitting the variational formulation for the governing equations into a coarse and a fine-scale part. The fine-scale part is then solved approximately to obtain the fine-scale solution model, that is substituted in the coarse-scale part of the variational formulation to obtain an upscaled problem. The authors have contributed to the development of the stochastic VMS method, wherein, algebraic models are used for the fine-scales and the GPCE

approach is used for representing stochastic quantities. The stochastic VMS formulation was tested against fluid flow and natural convection in the presence of uncertainty [32,33].

This paper is organized as follows: Section 2 provides some probability preliminaries followed by a brief discussion on Karhunen-Loève and generalized polynomial chaos expansions. The transient multiscale stochastic diffusion problem is defined in Section 3. This is followed by the definition of the VMS (operator upscaling approach), wherein, model equations are derived for the fine-scale solution. Finally, we derive the upscaled coarse formulation. Algorithmic issues involved in the implementation of the stochastic VMS approach are described in Section 4. In Section 5, we consider two numerical examples in order to investigate the stochastic VMS approach. Convergence studies and comparisons with a fully-resolved stochastic finite element solution are provided wherever possible. We finally conclude with a summary of the paper in Section 6.

2. The generalized polynomial chaos approach

In this section, we present some probability preliminaries, and a brief discussion on the Karhunen–Loève expansion (KLE) and the generalized polynomial chaos expansion (GPCE). For a considerably rigorous treatment of the above topics, the readers are referred to the original papers on the following: Stochastic finite elements and polynomial chaos [22–24,31,34], homogeneous chaos and theory behind spectral representation of uncertainty [35], generalized polynomial chaos approach [19,25,36,37] and the references therein.

2.1. Probability preliminaries

A complete probability space [38] is defined as the triple $(\Omega, \mathscr{F}, \mathscr{P})$, where Ω is the set of outcomes, $\mathscr{F}$ is the σ-algebra of subsets of Ω, and $\mathscr{P}$ is a probability measure that maps the σ-algebra to $[0,1]$. A random variable X is a function that maps Ω to a real interval $\mathbb{B}$, with a probability density function

$$f_X(x) := \frac{\mathrm{d}}{\mathrm{d}x}\mathscr{P}[X \leqslant x].$$

In this paper, we will denote a random variable X as $X(\omega)$, where $\omega \in \Omega$. The mathematical expectation [38] operator with respect to $X(\omega)$ is defined as

$$\mathbb{E}(X) := \int_\Omega X(\omega)\,\mathrm{d}\mathscr{P}(\omega) = \int_{\mathbb{B}} x f_X(x)\,\mathrm{d}x. \tag{1}$$

The complete function space $L_2(\Omega)$ can be defined as the set of all random variables that are mean-square integrable [38]. Incidentally, $L_2(\Omega)$ is also a Hilbert space with the inner product

$$(X, Y) := \mathbb{E}(\{X - \mathbb{E}(X)\}\{Y - \mathbb{E}(Y)\}), \quad X, Y \in L_2(\Omega). \tag{2}$$

Convergence in $L_2(\Omega)$ implies convergence in probability and convergence in distribution. As an extension of the above framework, a space-time stochastic process W defined on the spatial domain $\mathscr{D}$ and temporal domain $\mathscr{T}$ can be denoted as a function $W(\mathbf{x}, t, \omega)$. Theoretically, $W(\mathbf{x}, t, \omega)$ can be represented as a random variable at each spatial and temporal location, hence requiring an infinite number of random variables. For computational reasons, we are interested in a reduced-order representation of a stochastic process using a few random variables. Here, we briefly look at KLE and GPCE, two popular ways of representing an L_2 stochastic process as a spectral series expansion in orthonormal random variables. For a more detailed description, consult [22,25,33].

2.2. Karhunen–Loève expansion

The Karhunen–Loève expansion [20] is a technique for representing a L_2 stochastic process in a series expansion involving the eigenvalues and eigenfunctions of its covariance kernel as follows:

$$W(\mathbf{x}, t, \omega) = \mathbb{E}(W) + \sum_{i=1}^{\infty} \sqrt{\lambda_i} W_i(\mathbf{x}, t)\xi_i(\omega), \tag{3}$$

where $\mathbb{E}(W)$ is the mean of the stochastic process and $\xi_i(\omega)$ are appropriately defined orthonormal random variables [22]. The KLE generates uncorrelated random variables that can be orthonormalized. The eigenvalues λ_i and eigenfunctions $W_i(\mathbf{x}, t)$ are defined from the following eigenvalue problem:

$$\int_{\mathscr{D}\times\mathscr{T}} R_{WW}(\mathbf{x}_1, t_1, \mathbf{x}_2, t_2) W_i(\mathbf{x}_2, t_2)\, \mathrm{d}\mathbf{x}_2\, \mathrm{d}t_2 = \lambda_i W_i(\mathbf{x}_1, t_1), \tag{4}$$

where $R_{WW}(\mathbf{x}_1, t_1, \mathbf{x}_2, t_2)$ is the covariance function of $W(\mathbf{x}, t, \omega)$. The KLE is the optimal representation in mean-square sense. However, it requires the knowledge about the underlying stochastic process and its covariance kernel. Hence, the KLE is only used for representing the stochastic inputs. For more details, consult [22,31, and the references therein]. For computational purposes, the KLE is truncated to a finite number $(N+1)$ of expansion terms (including mean). Hence, the space-time stochastic process $W(\mathbf{x}, t, \omega)$ can be approximated using N random variables. In a typical stochastic input–output system with $W(\mathbf{x}, t, \omega)$ as the input, the KLE is used to represent the input in a series involving N orthonormal random variables. N, here is called the "KLE dimension" or the "input dimensionality". The output can now be represented as a function in space, time and the N orthonormal random variables. We will now describe the GPCE, a popular technique for representing the output.

2.3. Generalized polynomial chaos expansion

The GPCE is a technique for representing a L_2 stochastic process as a sum of its projections on an appropriately chosen basis of $L_2(\Omega)$. The original polynomial chaos comprised of Hermite polynomials in Gaussian random variables [35]. Cameron and Martin later proved that the polynomial chaos expansion converges to any L_2 stochastic process in mean-square sense [21]. Though the convergence rate of the original polynomial chaos is exponential for Gaussian and related processes (e.g. lognormal), the convergence rate is considerably slower for other types of processes (e.g. uniform and Gamma) [37].

In order to consider general random inputs, the GPCE uses orthogonal polynomials from the Askey scheme as a basis in $L_2(\Omega)$. Assuming that the stochastic input can be represented in a truncated KLE with N orthonormal random variables $\xi_1, \ldots, \xi_N$, in general, the GPCE of a space-time stochastic process (output) can be written in the following form [19,22]

$$W(\mathbf{x}, t, \omega) = \sum_{i=0}^{\infty} W_i(\mathbf{x}, t)\zeta_i(\omega), \tag{5}$$

where $\zeta_i(\omega)$ are hypergeometric orthogonal polynomials in $\xi_1(\omega), \ldots, \xi_N(\omega)$ from the Askey series such that their weighting functions equal the joint probability density function of the stochastic input e.g. if the stochastic input can be represented as a uniform random variable $\xi(\omega)$, then $\zeta_i(\omega)$ are Legendre polynomials in $\xi(\omega)$ [19,39] such that

$$\zeta_0 = 1, \quad \zeta_1 = \xi, \quad \zeta_2 = \frac{1}{2}(3\xi^2 - 1), \ldots.$$

Since each type of polynomial in the Askey scheme forms a complete basis of $L_2(\Omega)$, the convergence theorems of Cameron and Martin can be extended to the GPCE as well (consult [21,39] for an extensive overview). Again, for computational reasons, we often work with a truncated form of the GPCE.

Testing convergence of truncated GPCE: The truncated GPCE expansion of a stochastic process is characterized by two parameters viz. the dimension and order of the expansion. The dimension of the expansion is equal to the number of random variables used in the Karhunen–Loève expansion of the stochastic inputs. The order of the expansion is the highest order of Askey polynomials used in the GPCE. For example, a one-dimensional fourth-order Legendre chaos expansion implies that all one-dimensional Legendre polynomials up to fourth-order are included in the GPCE.

Since the accuracy of the truncated GPCE depends on the order of the expansion, we require techniques to determine the optimal truncation order. We use the weak-Cauchy convergence criterion for this purpose. The technique can be described as follows: assume that the dimension of the GPCE is known. Let the guess for optimal truncation order be q. Construct an order m GPCE, where $m = q + 1$, $q + 2$. The number of terms

(excluding mean) in the GPCE denoted here by $P(q)$ can be calculated as $(N+r)!/(N!r!)$, where N is the dimension and r is the order of the expansion. Using the above discussion, we can write the order q approximation and order m approximation as follows:

$$W^{(q)}(\mathbf{x},t,\theta)=\sum_{i=0}^{P(q)}W_i(\mathbf{x},t)\zeta_i(\omega),\quad W^{(m)}(\mathbf{x},t,\theta)=\sum_{i=0}^{P(m)}W_i(\mathbf{x},t)\zeta_i(\omega). \tag{6}$$

In the weak-Cauchy convergence criterion, we require that the L_2 norm of the difference in the two approximations be negligible, i.e.

$$E:=\|W^{(q)}-W^{(m)}\|_{L_2(\Omega)}<\epsilon,\quad 0<\epsilon\ll 1,\ \ m=q+1,q+2. \tag{7}$$

Note that the error measure E is a space-time function and that the above convergence should hold point-wise. These checks are made a priori in order to determine the optimal order of the GPCE. We note that though convergence in weak Cauchy sense is a good indicator of the convergence of the GPCE expansion, there are several other indicators that may have to be tested. For a survey of these convergence criteria, readers are referred to [40].

3. Mathematical model and variational multiscale method

3.1. Problem definition and variational formulation

Let $\mathscr{D}$, $\mathscr{T}$ and Ω denote a closed polygonal domain, a time interval and a suitable probability space, respectively. The transient diffusion in a heterogenous medium with a spatially varying random diffusion coefficient $k(\mathbf{x},\omega)$ can be written as the following stochastic partial differential equation (SPDE):

$$u_{,t}=\nabla\cdot(k(\mathbf{x},\omega)\nabla u)+f(\mathbf{x},t,\omega),\quad \mathbf{x}\in\mathscr{D},\ \ t\in\mathscr{T}\ \text{ and }\ \ \omega\in\Omega, \tag{8}$$

where, $u_{,t}$ denotes the partial time derivative $\partial u/\partial t$. The solution $u\equiv u(\mathbf{x},t,\omega)$ and the source term $f(\mathbf{x},t,\omega)$ are real-valued space-time stochastic fields. To simplify the presentation of our method, we further assume that the diffusion coefficient is isotropic.

For closure, we also assume the following initial and boundary conditions:

$$u(\mathbf{x},t,\omega)=u_g(\mathbf{x},t,\omega),\quad \mathbf{x}\in\partial\mathscr{D},\ \ t\in\mathscr{T}\ \text{ and }\ \omega\in\Omega, \tag{9}$$

$$u(\mathbf{x},0,\omega)=u_0(\mathbf{x},\omega),\quad \mathbf{x}\in\mathscr{D}\ \text{ and }\ \omega\in\Omega. \tag{10}$$

In order to introduce the variational form for Eqs. (8)–(10), we need to define the following function space [38,41]:

$$V_0=L_2(\Omega;L_2(\mathscr{T};H^1(\mathscr{D})))\stackrel{\text{def}}{=}\left\{v:\int_\Omega\int_{\mathscr{T}}\int_{\mathscr{D}}(v^2(\mathbf{x},t,\omega)+(\nabla v(\mathbf{x},t,\omega))^2)\,\mathrm{d}\mathscr{P}\,\mathrm{d}t\,\mathrm{d}\mathbf{x}<\infty\right\}.$$

Using the definition of V_0, the function space for the solution U and the trial function space V can now be defined as

$$U=\{u:u\in V_0,u=u_g,\mathbf{x}\in\partial\mathscr{D}\},\quad V=\{v:v\in V_0,v=0,\mathbf{x}\in\partial\mathscr{D}\}. \tag{11}$$

The variational formulation for Eqs. (8)–(10) can now be written as: find $u\in U$ such that for all $v\in V$

$$(u_{,t},v)+(k\nabla u,\nabla v)=(f,v), \tag{12}$$

where

$$(u,v)\stackrel{\text{def}}{=}\int_\Omega\int_{\mathscr{D}}uv\,\mathrm{d}\mathbf{x}\,\mathrm{d}\mathscr{P}. \tag{13}$$

3.2. Additive scale decomposition and variational multiscale method

In the variational multiscale approach, we consider the exact solution u to be made up of contributions from two different scales, namely, the coarse-scale solution u^{C}, that can be resolved using a coarse-mesh

and a subgrid solution u^{F}. In short, $u = u^{\mathrm{C}} + u^{\mathrm{F}}$ (consult [15,29,30,42] for further details). This additive sum decomposition induces a similar decomposition for the function spaces as $U = U^{\mathrm{C}} \oplus U^{\mathrm{F}}$ and $V = V^{\mathrm{C}} \oplus V^{\mathrm{F}}$, respectively. Typically, the coarse-scale function spaces U^{C} and V^{C} are finite dimensional and are characterized by piecewise polynomials defined on a coarse-mesh.

The main idea behind the VMS (operator upscaling) method is to develop models for characterizing the effect of the subgrid solution on the coarse-scale solution and to subsequently derive a modified coarse-scale formulation that only involves u^{C} [32,42,43]. In order to do that, we split the variational formulation given in Eq. (12) as the following coarse-scale and subgrid equations: Find $u^{\mathrm{C}} \in U^{\mathrm{C}}$ and $u^{\mathrm{F}} \in U^{\mathrm{F}}$ such that

$$(u^{\mathrm{C}}_{,t} + u^{\mathrm{F}}_{,t}, v^{\mathrm{C}}) + (k\nabla u^{\mathrm{C}} + k\nabla u^{\mathrm{F}}, \nabla v^{\mathrm{C}}) = (f, v^{\mathrm{C}}) \quad \forall v^{\mathrm{C}} \in V^{\mathrm{C}}, \tag{14}$$

$$(u^{\mathrm{C}}_{,t} + u^{\mathrm{F}}_{,t}, v^{\mathrm{F}}) + (k\nabla u^{\mathrm{C}} + k\nabla u^{\mathrm{F}}, \nabla v^{\mathrm{F}}) = (f, v^{\mathrm{F}}) \quad \forall v^{\mathrm{F}} \in V^{\mathrm{F}}. \tag{15}$$

We will now proceed to solve Eq. (15) by applying localization assumptions to obtain an approximate model for the subgrid solution u^{F}. Subsequently, we will use the model for subgrid solution to eliminate u^{F} in Eq. (14) to obtain a modified formulation defined only in terms of u^{C}.

3.3. Subgrid modeling

Assume that the spatial domain is discretized using a coarse-mesh into disjoint sub-domains $\mathscr{D}^{(e)}, e = 1, \ldots, \mathrm{Nel}$, where, (e) denotes the sub-domain number. We will refer to these sub-domains as "coarse elements". Let each coarse element be further discretized using a subgrid mesh into "$\mathrm{Nel}^{\mathrm{F}}_{(e)}$" disjoint sub-domains (also referred to as "subgrid elements").

As considered in [3,4,7,8], we will now assume that the subgrid solution is a sum of two components $\hat{u}^{\mathrm{F}}$ and u^{F0} that obey the following variational equations:

$$(u^{\mathrm{C}}_{,t}, v^{\mathrm{F}}) + (\hat{u}^{\mathrm{F}}_{,t}, v^{\mathrm{F}}) + (k\nabla u^{\mathrm{C}}, \nabla v^{\mathrm{F}}) + (k\nabla \hat{u}^{\mathrm{F}}, \nabla v^{\mathrm{F}}) = 0, \tag{16}$$

$$(u^{\mathrm{F0}}_{,t}, v^{\mathrm{F}}) + (k\nabla u^{\mathrm{F0}}, \nabla v^{\mathrm{F}}) = (f, v^{\mathrm{F}}), \tag{17}$$

where $\hat{u}^{\mathrm{F}}$ incorporates entire coarse-scale solution information and u^{F0} is independent of the coarse-scale solution. The dynamics of u^{F0} is driven by the projection of the source term $f(\mathbf{x}, t, \omega)$ onto the subgrid trial function space V^{F}.

By Eq. (16), the term $\hat{u}^{\mathrm{F}}$ behaves as a mapping from coarse-scale solution to the subgrid solution. Hence, we refer to $\hat{u}^{\mathrm{F}}$ as the coarse-to-subgrid (C2S) map. Owing to the affine nature of Eq. (17), we shall refer to u^{F0} as the affine correction term.

In the current form, Eqs. (16) and (17) are defined over the entire spatial domain and are exact. Hence, their numerical simulations possess the same computational requirement as the fully-resolved problem (fine-mesh and small time-stepping). In order to localize the calculations of the subgrid solution, we will consider restrictions of Eqs. (16) and (17) to each coarse element $\mathscr{D}^{(e)}$. This restriction can be written as follows: Find $\hat{u}^{\mathrm{F}} \in U^{(e)}$ and $u^{\mathrm{F0}} \in U^{(e)}_0$ such that for all $v \in V^{(e)}$, Eqs. (16) and (17) hold. The function spaces $U^{(e)}$ and $U^{(e)}_0$ are restrictions of V_0 to the coarse element $\mathscr{D}^{(e)}$ with suitable boundary conditions. The derivations in subsequent sections are performed for a single coarse element $\mathscr{D}^{(e)}$.

3.4. C2S map and multiscale basis functions

Let us assume that in a fully-resolved direct numerical simulation, the dynamics of the exact solution can be captured using a fine time-step of δt. Since the length scales of interest in the coarse solution are far greater than the smallest length scale in the exact solution, we assume that the coarse time-step Δt is much larger in comparison to δt [44–46]. Let us consider a coarse time-step $\Delta t = [t_n, t_n + 1]$. Let t' be the local time coordinate defined such that at t_n, $t' = 0$ and at $t_n + 1$, $t' = \Delta t$.

Let us also assume a piecewise polynomial finite element representation for the coarse solution inside a coarse element $\mathscr{D}^{(e)}$ (please note that (e) is suppressed henceforth to simplify notation):

$$u^{\mathrm{C}}(\mathbf{x},t,\omega)=\sum_{\beta=1}^{\mathrm{Nbf}}u^{\mathrm{C}}_{\beta}(t',\omega)\Psi_{\beta}(\mathbf{x}), \tag{18}$$

where Nbf denotes the number of finite-element shape functions (piecewise polynomials) defined on the coarse element [32,33]. Let us further assume a truncated generalized polynomial chaos expansion with $P_{\mathrm{C}}+1$ terms for each of the coefficients $u^{\mathrm{C}}_{\beta}(t',\omega)$

$$u^{\mathrm{C}}_{\beta}(t',\omega)=\sum_{s=0}^{\mathrm{P_C}}u^{\mathrm{C}}_{\beta s}(t')\zeta_s(\omega). \tag{19}$$

Thus, the stochastic finite-element (spatial finite-element + GPCE) representation of the coarse solution can be written using local time coordinate as

$$u^{\mathrm{C}}(\mathbf{x},t,\omega)=\sum_{\beta=1}^{\mathrm{Nbf}}\sum_{s=0}^{\mathrm{P_C}}u^{\mathrm{C}}_{\beta s}(t')\zeta_s(\omega)\Psi_{\beta}(\mathbf{x}), \tag{20}$$

where $u^{\mathrm{C}}_{\beta s}(t')$ denotes the nodal solution (each node has $P_{\mathrm{C}}+1$ degrees of freedom) and $\zeta_s(\omega)$ are polynomials from the hypergeometric Askey series. The form of Eq. (20) has been used in our earlier works [32,33].

Note: We have represented the left hand side of Eqs. (18) and (20) as a function of the global time coordinate t and the right hand side as a function of the local time coordinate t' with a tacit understanding that t and t' are related as $t'=t-t_n$ in the interval $t\in[t_n,t_{n+1}]$.

For the C2S map $\hat{u}^{\mathrm{F}}$, we seek a representation similar to Eq. (20) based on Green's function theory [8]

$$\hat{u}^{\mathrm{F}}(\mathbf{x},t,\omega)=\sum_{\beta=1}^{\mathrm{Nbf}}\sum_{s=0}^{\mathrm{P_C}}u^{\mathrm{C}}_{\beta s}(t')\phi^{\mathrm{F}}_{\beta s}(\mathbf{x},t',\omega). \tag{21}$$

The fine-scale variational formulation of Eq. (16) can be re-written after substitution of Eqs. (20) and (21) as follows:

$$(u^{\mathrm{C}}_{\beta s,t}\zeta_s\Psi_{\beta},v^{\mathrm{F}})+(u^{\mathrm{C}}_{\beta s,t}\phi^{\mathrm{F}}_{\beta s}+u^{\mathrm{C}}_{\beta s}\phi^{\mathrm{F}}_{\beta s,t},v^{\mathrm{F}})+(ku^{\mathrm{C}}_{\beta s}\nabla\phi^{\mathrm{F}}_{\beta s},\nabla v^{\mathrm{F}})+(ku^{\mathrm{C}}_{\beta s}\nabla\Psi_{\beta}\zeta_s,\nabla v^{\mathrm{F}})=0, \tag{22}$$

where the repeated indices β and s indicate a summation over $1,\ldots,\mathrm{Nbf}$ and $0,\ldots,P_{\mathrm{C}}$, respectively (with similar notation applied to subsequent equations as well). Also, for clarity of presentation, the dependence on $\mathbf{x}$, t and ω is not shown in the expressions for $\Psi_{\beta}(\mathbf{x}),\zeta_s(\omega),\phi^{\mathrm{F}}_{\beta s}(\mathbf{x},t',\omega)$ and $k(\mathbf{x},\omega)$. The above equation can be further simplified as follows:

$$(\{u^{\mathrm{C}}_{\beta s}(\zeta_s\Psi_{\beta}+\phi^{\mathrm{F}}_{\beta s})\}_{,t},v^{\mathrm{F}})+(k\nabla\{u^{\mathrm{C}}_{\beta s}(\zeta_s\Psi_{\beta}+\phi^{\mathrm{F}}_{\beta s})\},\nabla v^{\mathrm{F}})=0. \tag{23}$$

For a deterministic analog of the above equation, the readers are referred to [42].

Without loss of generality, we can assume the following representation for the coarse-scale nodal solutions $u^{\mathrm{C}}_{\beta s}(t')$ inside the coarse time-step

$$u^{\mathrm{C}}_{\beta s}(t')=A(t')\tilde{u}^{\mathrm{C}}_{\beta s}+B(t')\bar{u}^{\mathrm{C}}_{\beta s}, \tag{24}$$

where $\tilde{u}^{\mathrm{C}}_{\beta s}$ and $\bar{u}^{\mathrm{C}}_{\beta s}$ denote the nodal coefficients in the GPCE of the coarse solution at the start and end of the coarse time step (see Fig. 1). $A(t')$ and $B(t')$ are special positive functions that obey the following relations:

$$A(t')+B(t')=1,\quad A(0)=1,\quad A(\Delta t)=0,\quad B(0)=0,\quad \text{and}\quad B(\Delta t)=1. \tag{25}$$

Eq. (24) involves representation of a function as a convex combination of two functions [41].

The representation given in Eq. (24) is quite general and incorporates several well-known time integration rules. For example, $A(t')=(\Delta t-t')/\Delta t$ and $B(t')=t'/\Delta t$ yields a backward-Euler time integration rule.

From Eqs. (21) and (24), we can write the C2S map as follows:

$$\hat{u}^{\mathrm{F}}_{\beta s}(\mathbf{x},t,\omega)=\sum_{\beta=1}^{\mathrm{Nbf}}\sum_{s=0}^{P_{\mathrm{C}}}[\tilde{u}^{\mathrm{C}}_{\beta s}A(t')\phi^{\mathrm{F}}_{\beta s}(\mathbf{x},t',\omega)+\bar{u}^{\mathrm{C}}_{\beta s}B(t')\phi^{\mathrm{F}}_{\beta s}(\mathbf{x},t',\omega)]. \tag{26}$$

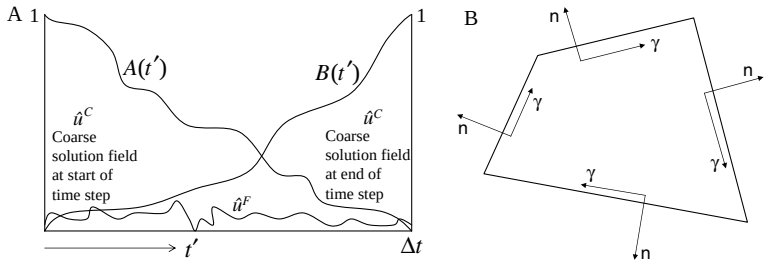

Fig. 1. (A) Schematic of the time integration framework: Δt is the coarse-time step and t' is the local time coordinate. The integration parameters $A(t')$ and $B(t')$ are shown in the figure. Also, $\tilde{u}^{\mathrm{C}}_{\beta s}$ and $\bar{u}^{\mathrm{C}}_{\beta s}$ are identified as the coarse solution fields at the start and end of the coarse time step, respectively. (B) Schematic of a typical coarse element sub-domain: The coordinates normal and tangential to the element edges are denoted by the letters n and γ, respectively.

We can now write Eq. (23) as

$$\tilde{u}^{\mathrm{C}}_{\beta s}\{(\{A(t')(\zeta_s\Psi_\beta+\phi^{\mathrm{F}}_{\beta s})\}_{,t},v^{\mathrm{F}})+(k\nabla\{A(t')(\zeta_s\Psi_\beta+\phi^{\mathrm{F}}_{\beta s})\},\nabla v^{\mathrm{F}})\}+\bar{u}^{\mathrm{C}}_{\beta s}\{(\{B(t')(\zeta_s\Psi_\beta+\phi^{\mathrm{F}}_{\beta s})\}_{,t},v^{\mathrm{F}}) + (k\nabla\{B(t')(\zeta_s\Psi_\beta+\phi^{\mathrm{F}}_{\beta s})\},\nabla v^{\mathrm{F}})\}=0. \tag{27}$$

Note that the above equation is fully characterized based on the values taken by $\tilde{u}^{\mathrm{C}}_{\beta s}$ and $\bar{u}^{\mathrm{C}}_{\beta s}$ and the subgrid basis function $\phi^{\mathrm{F}}_{\beta s}$.

We are looking to construct a localized scheme for representation of the subgrid solutions. Further, this localized scheme should hold for all possible values of the coarse nodal coefficients $\tilde{u}^{\mathrm{C}}_{\beta s}$ and $\bar{u}^{\mathrm{C}}_{\beta s}$. Hence, we equate the terms in parentheses to zero to obtain the following set of variational formulations defined for each combination of indices β and s, where, $\beta=1,\ldots,\mathrm{Nbf}$ and $s=0,\ldots,P_{\mathrm{C}}$:

$$(\{A(t')(\zeta_s\Psi_\beta+\phi^{\mathrm{F}}_{\beta s})\}_{,t},v^{\mathrm{F}})+(k\nabla\{A(t')(\zeta_s\Psi_\beta+\phi^{\mathrm{F}}_{\beta s})\},\nabla v^{\mathrm{F}})=0, \tag{28}$$

$$(\{B(t')(\zeta_s\Psi_\beta+\phi^{\mathrm{F}}_{\beta s})\}_{,t},v^{\mathrm{F}})+(k\nabla\{B(t')(\zeta_s\Psi_\beta+\phi^{\mathrm{F}}_{\beta s})\},\nabla v^{\mathrm{F}})=0. \tag{29}$$

Now, by using the relations $A(t')+B(t')=1$, we can simplify Eq. (29) as follows:

$$((\zeta_s\Psi_\beta+\phi^{\mathrm{F}}_{\beta s})_{,t},v^{\mathrm{F}})+(k\nabla(\zeta_s\Psi_\beta+\phi^{\mathrm{F}}_{\beta s}),\nabla v^{\mathrm{F}}) - (\{A(t')(\zeta_s\Psi_\beta+\phi^{\mathrm{F}}_{\beta s})\}_{,t},v^{\mathrm{F}})-(k\nabla\{A(t')(\zeta_s\Psi_\beta+\phi^{\mathrm{F}}_{\beta s})\},\nabla v^{\mathrm{F}})=0. \tag{30}$$

By combining Eqs. (28) and (30), we obtain the evolution equation for $\phi^{\mathrm{F}}_{\beta s}$

$$((\zeta_s\Psi_\beta+\phi^{\mathrm{F}}_{\beta s})_{,t},v^{\mathrm{F}})+(k\nabla(\zeta_s\Psi_\beta+\phi^{\mathrm{F}}_{\beta s}),\nabla v^{\mathrm{F}})=0. \tag{31}$$

Remark 1. The C2S map is completely characterized given the coarse-scale nodal solution coefficients $u^{\mathrm{C}}_{\beta s}(t')$ and $\phi^{\mathrm{F}}_{\beta s}(\mathbf{x},t',\omega)$ (in turn obtained by solving Eq. (31) for each combination of indices β and s).

3.5. Boundary conditions for subgrid basis functions

In order to localize the computation of $\hat{u}$ to a coarse element, we need an approximate specification of its boundary conditions along coarse-element edges.

By assuming twice-differentiability of the subgrid basis functions, we can write the strong formulation for Eq. (31) as: find $\phi^{\mathrm{F}}_{\beta s}$ for $\mathbf{x}\in\mathscr{D}^{(\mathrm{e})}$ and $t\in[t_n,t_{n+1}]$ such that

$$\phi^{\mathrm{F}}_{\beta s,t}-\nabla\cdot(k(\mathbf{x},\omega)\nabla\phi^{\mathrm{F}}_{\beta s})-\nabla\cdot(k(\mathbf{x},\omega)\nabla\Psi_\beta(\mathbf{x})\zeta_s(\omega))=0. \tag{32}$$

Notice that the above equation contains $\nabla\cdot(k(\mathbf{x},\omega)\nabla\Psi_\beta(\mathbf{x})\zeta_s(\omega))$ as a source term, whose computation can be avoided by defining a new variable $\Phi_{\beta s}$

$$\Phi_{\beta s}(\mathbf{x}, t', \omega) = \Psi_\beta(\mathbf{x})\zeta_s(\omega) + \phi^{\mathrm{F}}_{\beta s}(\mathbf{x}, t', \omega), \tag{33}$$

It can be shown that $\Phi_{\beta s}$ satisfies the following equation

$$\Phi_{\beta s,t} - \nabla \cdot (k(\mathbf{x}, \omega)\nabla \Phi_{\beta s}) = 0. \tag{34}$$

In order to complete the specification of this equation, we need to specify boundary conditions for $\Phi_{\beta s}$ on the coarse-element boundaries $\partial\mathscr{D}^{(e)}$. We extend ideas from the multiscale finite element method [1] that indicate that the behavior of $\Phi_{\beta s}$ on the boundaries of the coarse element should retain the characteristics of Eq. (34). Here, we use the Dirichlet boundary condition $\Phi_{\beta s} = \Phi^{\Gamma}_{\beta s}$ on the coarse element boundary, where, $\Phi^{\Gamma}_{\beta s}$ satisfies the following reduced partial differential equation for computation from t_n to $t_n + 1$ $(n = 0, 1, \ldots)$.

$$\Phi^{\Gamma}_{\beta s,t}(\mathbf{x}, t', \omega) - \frac{\partial}{\partial\gamma}\left(k(\mathbf{x}, \omega)\frac{\partial \Phi^{\Gamma}_{\beta s}}{\partial\gamma}\right) = 0, \quad \mathbf{x} \in \partial\mathscr{D}^{(e)}, \tag{35}$$

$$\Phi^{\Gamma}_{\beta s}(\mathbf{x}_\alpha, t', \omega) = \delta_{\alpha\beta}\zeta_s(\omega), \tag{36}$$

$$\Phi^{\Gamma}_{\beta s}(\mathbf{x}, 0, \omega) = \Phi^{\Gamma}_{\beta s}(\mathbf{x}, t_n, \omega), \quad \mathbf{x} \in \partial\mathscr{D}^{(e)}, \ \ t = t_n, \tag{37}$$

where γ is the coordinate used to parameterize the boundary of the coarse element and $\mathbf{x}_\alpha$ denotes the vertex of the coarse element $\mathscr{D}^{(e)}$ where the coarse finite-element basis function Ψ_α takes the value unity. A schematic showing the calculation of boundary subgrid basis functions for the case of a quadrilateral coarse element is shown in Fig. 1.

Remark 2. The above specification of boundary conditions for the subgrid basis function is restricted to polygonal coarse element shapes (quadrilateral, triangles and other).

Let us assume that the subgrid function space V^{F} can be represented as the tensor product space obtained by combining the space of finite-element basis functions defined on the subgrid mesh $[N_\beta(\mathbf{x}), \beta = 1, \ldots, \mathrm{Nbf}]$ and Askey polynomials $[\zeta_r(\omega), r = 0, \ldots, P_{\mathrm{F}}]$. We emphasize that the number of terms required for the GPCE of the subgrid basis functions to converge can be different than P_{C}, the number of terms used in the discretization of the coarse solution.

We can now express the variational form for Eq. (34) as a matrix–vector equation defined in each coarse element as follows (for details regarding stochastic finite element solution of a diffusion equation, consult [47]):

$$[M]\{\Phi^{\mathrm{F}}_{\beta s,t}\} + [K]\{\Phi^{\mathrm{F}}_{\beta s}\} = 0, \tag{38}$$

where $[M(t)]$, $[K(t)]$ are defined as follows:

$$[\mathrm{M}] = (N_\beta\zeta_s, N_\alpha\zeta_r), \tag{39}$$

$$[\mathrm{K}] = (k\nabla N_\beta\zeta_s, \nabla N_\alpha\zeta_r), \tag{40}$$

and $\{\Phi^{\mathrm{F}}_{\beta s}\}$ represent the nodal values of the subgrid basis function defined on the subgrid mesh in each coarse element.

3.6. Affine correction term

The affine correction term u^{F0} as defined by Eq. (17) leads to the following strong form of equations inside each coarse element sub-domain

$$u^{\mathrm{F0}}_{,t} + \nabla \cdot (k\nabla u^{\mathrm{F0}}) = f, \quad \mathbf{x} \in \mathscr{D}^{(e)}. \tag{41}$$

Burn-in time for VMS simulations: Before proceeding to specify boundary conditions for the affine correction term, it is necessary to understand its origin as a sum of two contributions, namely, the effect of sources and sinks at the subgrid level and the effect of the subgrid component of the initial condition $u(\mathbf{x}, 0, \omega) = u_0(\mathbf{x}, \omega)$. Typically, the latter effect is global and the present algorithm does not allow its treatment. However, the effect of the subgrid component of the initial condition tends to decay with time. Thus, in the VMS simulation, the subgrid basis functions are generated up to a cutoff time (referred here as the

burn-in time) that is chosen such that the effects of the subgrid component of the initial condition do not affect the coarse solution. This also ensures that the subgrid basis functions capture sufficient information about the heterogeneities at the subgrid scale. Thus, whenever the affine correction term is mentioned, it implies only the effects of sources and sinks at the subgrid level.

Boundary conditions for the affine correction term: Note that the affine correction term does not have any coarse-scale solution dependence, hence, the assumption that this term goes to zero on coarse element boundaries is justified i.e. $u^{\mathrm{F0}} = 0$ on coarse element boundaries. Furthermore, we assume that the affine correction is zero at the start of each coarse time-step i.e. $u^{\mathrm{F0}}(\mathbf{x}, 0, \omega) = 0$ (note that the initial conditions here refer to the local time coordinate t'=0).

Remark 3. If the coarse-time step is large enough or if the source terms do not have rapid variations in time, the affine correction term can be assumed to be quasi-static ($u^{\mathrm{F0}}_{,t} = 0$). This assumption drastically reduces the computation time with little loss of accuracy. Also, if the source term is zero and the exact initial conditions do not have excessive fine-scale fluctuations, we can assume that the affine correction is identically zero.

3.7. Modified coarse-scale formulation

We can now substitute $\Phi_{\beta s}$ and u^{F0} in the coarse-scale variational formulation given in Eq. (14) to obtain the following: In each coarse element $\mathscr{D}^{(e)}$,

$$(u^{\mathrm{C}}_{\beta s,t}\Phi_{\beta s}, v^{\mathrm{C}}) + (u^{\mathrm{C}}_{\beta s}\Phi_{\beta s,t}, v^{\mathrm{C}}) + (u^{\mathrm{C}}_{\beta s}k\nabla\Phi_{\beta s}, \nabla v^{\mathrm{C}}) = (f, v^{\mathrm{C}}) - (k\nabla u^{\mathrm{F0}}, \nabla v^{\mathrm{C}}) - (u^{\mathrm{F0}}_{,t}, v^{\mathrm{C}}). \tag{42}$$

Thus, the affine correction term figures in the modified coarse-scale variational formulation as a sum of two terms: an anti-diffusive term and a term involving its time derivative [3,4,7].

By choosing V^{C} as the tensor product space obtained by combining the space of coarse element basis functions $[\Psi_\beta(\mathbf{x}), \beta = 1, \ldots, \mathrm{Nbf}]$ and Askey polynomials $[\zeta_r(\omega), r = 0, \ldots, P_{\mathrm{C}}]$, we can express Eq. (42) as a matrix–vector equation on each coarse element $\mathscr{D}^{(e)}$

$$[M(t)]\{u^{\mathrm{C}}_{,t}\} + [K(t)]\{u^{\mathrm{C}}\} = \{f(t)\}, \tag{43}$$

where the dependence of $[M(t)]$, $[K(t)]$ and $\{f(t)\}$ on time comes from the basis functions $\Phi_{\beta s}$ and the time varying source term $f(\mathbf{x}, t, \omega)$, respectively as follows:

$$\begin{aligned}
[M] &= (\Phi_{\beta s}(\mathbf{x}, t', \omega)\Psi_\alpha(\mathbf{x})\zeta_r(\omega)),\\
[K] &= (k(\mathbf{x}, \omega)\nabla\Phi_{\beta s}(\mathbf{x}, t', \omega), \nabla\Psi_\alpha(\mathbf{x})\zeta_r(\omega)) + (\Phi_{\beta s,t}(\mathbf{x}, t', \omega), \Psi_\alpha(\mathbf{x})\zeta_r(\omega)),\\
\{f\} &= (f(\mathbf{x}, t, \omega), \Psi_\alpha(\mathbf{x})\zeta_r(\omega)) - (u^{\mathrm{F0}}_{,t}(\mathbf{x}, t', \omega), \Psi_\alpha(\mathbf{x})\zeta_r(\omega))\\
&\quad - (k(\mathbf{x}, \omega)\nabla u^{\mathrm{F0}}(\mathbf{x}, t', \omega), \nabla\Psi_\alpha(\mathbf{x})\zeta_r(\omega)),
\end{aligned} \tag{44}$$

and $\{u^{\mathrm{C}}\}$ represent the nodal values of the coarse solution in each coarse element i.e. the coefficients $u^{\mathrm{C}}_{\beta s}$ defined in Eq. (20).

Remark 4. Since, each node requires $P_{\mathrm{C}} + 1$ generalized polynomial chaos coefficients for the representation of the coarse solution, we have $P_{\mathrm{C}} + 1$ degrees of freedom per node in the coarse-mesh. Also, the matrices $[M(t)]$, $[K(t)]$ and the vector $\{f(t)\}$ have terms that contain dynamics happening at the subgrid scale, hence, in order to reduce computation time, we need to apply some time averaging scheme such that the matrices and force vector can be written exclusively in terms of the coarse time-step. In this paper, we use a backward-Euler time integration rule for the coarse solution, hence, the following scheme is adopted in time-stepping from t_n to $t_n + 1$ (where $\Delta t = t_n + 1 - t_n$).

$$([M(t_n + 1)] + \Delta t[K(t_n + 1)])\{u^{\mathrm{C}}(t_n + 1)\} = \Delta t\{f(t_n + 1)\} + [M(t_n)]\{u^{\mathrm{C}}(t_n)\}. \tag{45}$$

The effect of using the approximate coarse-scale implementation given in Eq. (45) is currently determined by comparison with the fully-resolved simulation. Further studies are required in this context.

4. Computational issues

4.1. Special structure of subgrid problems

According to Eq. (34), in order to generate the subgrid basis functions, we need to solve $\mathrm{Nbf}(P_C + 1)$ stochastic PDEs in each coarse element. However, a close observation of the structure of the subgrid problems reveals that by just solving Nbf problems (defined for the basis function $\Phi_{\beta 0}$, $\beta = 1, \ldots, \mathrm{Nbf}$) in each coarse element, we can generate the remaining subgrid basis functions using the following relations:

$$\Phi_{\beta s}(\mathbf{x}, t', \omega) = \Phi_{\beta 0}(\mathbf{x}, t', \omega)\zeta_s(\omega). \tag{46}$$

By substituting the above relation, Eqs. (34)–(37) are satisfied identically assuming that the governing equations and boundary conditions for $\Phi_{\beta 0}$ in each coarse element are as follows

$$\Phi_{\beta 0}(\mathbf{x}, t', \omega) - \nabla \cdot (k(\mathbf{x}, \omega)\nabla \Phi_{\beta 0}(\mathbf{x}, t', \omega)) = 0, \quad \mathbf{x} \in \mathscr{D}^{(e)}, \tag{47}$$

where $\Phi_{\beta 0}$ satisfies the following reduced differential equation on the coarse element boundary (parameterized here by the coordinate γ, see Fig. 1).

$$\begin{aligned}
&\Phi^{\Gamma}_{\beta 0,t}(\mathbf{x}, t', \omega) - \frac{\partial}{\partial \gamma}\left(k(\mathbf{x}, \omega)\frac{\partial \Phi^{\Gamma}_{\beta 0}}{\partial \gamma}\right) = 0, \quad \mathbf{x} \in \partial\mathscr{D}^{(e)},\\
&\Phi^{\Gamma}_{\beta 0}(\mathbf{x}_\alpha, t', \omega) = \delta_{\alpha\beta},\\
&\Phi^{\Gamma}_{\beta 0}(\mathbf{x}, 0, \omega) = \Psi_\beta(\mathbf{x}), \mathbf{x} \in \partial\mathscr{D}^{(e)}, \quad t = 0,\\
&\qquad\qquad = \Phi^{\Gamma}_{\beta 0}(\mathbf{x}, t_n, \omega), \mathbf{x} \in \partial\mathscr{D}^{(e)}, \quad t = t_n.
\end{aligned}$$

Remark 5. As a special case, if the diffusion coefficient is periodic with period L, we can choose the coarse element width to be a multiple of L. It can be shown that the subgrid basis functions are the same for all coarse elements. This enables us to achieve tremendous reduction in memory storage and computational cost since we can calculate and store the subgrid solution for a single coarse element and re-use it for element matrix–vector calculations. However, we emphasize that our approach does not require periodicity.

4.2. Quasistatic subgrid solution

In many practical problems of interest, the assumption of a quasistatic subgrid solution is fairly accurate, i.e. in the governing equations for subgrid basis functions $\Phi_{\beta 0}$, we assume that $\Phi_{\beta 0,t} \approx 0$. This further reduces the computational cost since, the subgrid basis functions can be computed once and for all at the start of the computation and also, the memory required to store stationary subgrid basis is far less than that for storing subgrid dynamics.

4.3. Post-processing: fine-scale solution reconstruction

Let us assume that the coarse-scale solution, the subgrid basis functions and the affine-correction at a particular time-step are $u^{\mathrm{C}}(\mathbf{x}, \omega)$, $\Phi_{\beta 0}(\mathbf{x}, \omega)$ and $u^{\mathrm{F0}}(\mathbf{x}, \omega)$, respectively. The time dependence is not shown here for clarity sake. Also, we emphasize that all calculations in this section are performed on the subgrid mesh associated with each coarse element $\mathscr{D}^{(e)}$.

Inside a given coarse element $\mathscr{D}^{(e)}$, we calculate the reconstructed fine-scale VMS solution as follows:

$$u = \sum_{\beta=1}^{\mathrm{Nbf}} \sum_{s=0}^{P_C} u^{\mathrm{C}}_{\beta s}\Phi_{\beta s} + u^{\mathrm{F0}}(\mathbf{x}, \omega), \tag{48}$$

where $\Phi_{\beta s} = \phi^{\mathrm{F}}_{\beta s} + \Psi_\beta \zeta_s$, is the sum of coarse and subgrid basis functions defined on $\mathscr{D}^{(e)}$. Let us now consider the GPCE expansions for $\Phi_{\beta s}$ (after substituting Eq. (46)) and u^{F0} as follows:

$$\Phi_{\beta s} = \Phi_{\beta 0}\zeta_s = \sum_{r=0}^{P_F} \Phi_{\beta 0 r}\zeta_s\zeta_r, \quad u^{\mathrm{F0}} = \sum_{r=0}^{P_F} u^{\mathrm{F0}}_r \zeta_r, \tag{49}$$

wherein $P_F + 1$ is the number of terms used in the GPCE expansion of $\Phi_{\beta 0}$ and u^{F0}. Now, we can write Eq. (48) as follows:

$$u = \sum_{\beta=1}^{\mathrm{Nbf}} \sum_{s=0}^{P_C} \sum_{r=0}^{P_F} u^{\mathrm{C}}_{\beta s} \Phi_{\beta 0 r}(\mathbf{x})\zeta_r(\omega)\zeta_s(\omega) + \sum_{r=0}^{P_F} u^{\mathrm{F0}}_r(\mathbf{x})\zeta_r(\omega), \quad \mathbf{x} \in \mathscr{D}^{(e)}. \tag{50}$$

The mth term in the GPCE of the reconstructed fine-scale VMS solution u can now be written as follows:

$$u_m = \sum_{\beta=1}^{\mathrm{Nbf}} \sum_{s=0}^{P_C} \sum_{r=0}^{P_F} u^{\mathrm{C}}_{\beta s} \Phi_{\beta 0 r} \frac{\langle \zeta_r(\omega)\zeta_s(\omega)\zeta_m(\omega)\rangle}{\langle \zeta_m(\omega)\zeta_m(\omega)\rangle} + u^{\mathrm{F0}}_m(\mathbf{x}), \tag{51}$$

where $\langle f(\omega)\rangle$ is used to denote the mathematical expectation of the random function $f(\omega)$.

Notice that the construction of the fully-resolved fine-scale solution is just a post-processing step. In actual computation, we just need to store the subgrid basis functions, the affine correction and the coarse-scale term.

Note: Henceforth, in Section 5, we will denote P_{C} as the coarse-scale GPCE order and P_{F} as the fine-scale GPCE order.

Comparison of the reconstructed VMS fine-scale solution with a fully-resolved stochastic FEM solution: Assume that the reconstructed fine-scale VMS solution (see Eq. (51)) and the fully-resolved stochastic finite element solution be represented in their respective GPCEs as follows:

$$U^{\mathrm{vms}} = \sum_{i=0}^{P} U^{\mathrm{vms}}_i \zeta_i(\omega); \text{ and } U^{\mathrm{fem}} = \sum_{i=0}^{P} U^{\mathrm{fem}}_i \zeta_i(\omega). \tag{52}$$

We define the upscaling L_2 error measures with respect to each GPCE coefficient as follows:

$$E_i := \|U^{\mathrm{vms}}_i - U^{\mathrm{fem}}_i\|_{L_2(\mathscr{D})}. \tag{53}$$

Note that the error is defined with respect to spatial domain only. The above error measure is not unique and in certain circumstances, it is important to consider other error measures (consult [40] for a comprehensive survey).

5. Numerical examples

Unless otherwise specified, all computations in this section are performed on a $[0,1]\times[0,1]$ square domain. Bilinear quadrilateral elements are used for spatial finite element interpolation and a Legendre-chaos is used for representation of output in its GPCE (note that Legendre-chaos is the optimal representation for input with a uniform probability distribution) [19,32,25].

In this section, we solve two examples with different uncertainty models. In Example I, we explicitly consider a scale separation in the model for diffusion coefficient, such that the coarse length scale is of order 1 and the fine length scale is a random combination of the parameters ϵ_0 and ϵ_1. In the second example, there is no explicit length scale for the coarse and fine-scale solutions (diffusion in microstructures). In particular, we consider a two phase microstructure where the uncertainty in the diffusion coefficient is due to lack of precise knowledge of the diffusion coefficients of its constituents.

Also, the purpose of each example is different. In Example I, we study the behavior of the reconstructed fine-scale VMS solution for the dynamic subgrid assumption, the effect of quasistatic subgrid assumption on upscaling accuracy, and the shortcomings in the dynamic subgrid model with respect to subgrid boundary condition and initial condition models (see Section 3.6). In Example II, we provide a comparison of the fully-resolved stochastic finite element solution with the reconstructed fine-scale VMS solution with a quasistatic subgrid assumption, and the coarse-scale VMS solution.

We use a fully-resolved GPCE simulation of the diffusion equation to obtain the reference solution for comparison with the upscaled VMS solutions. We note that the GPCE based stochastic finite element implementation for the stochastic diffusion equation has been implemented and tested against Monte Carlo and other analytical solutions by the authors [47] and others [39,48].

Remark 6. In both examples, we use an important assumption that the diffusion coefficient can be represented using a few random variables (one in Example I and two in Example II). This is crucial to the success of GPCE formulations wherein, the number of terms required for convergence in the GPCE increases exponentially with the number of input random variables [22,37]. If the diffusion coefficient has short range variability and subsequently a steeply decaying covariance kernel, then Monte-Carlo is the only way for uncertainty analysis [26,25].

5.1. Example I: transient diffusion in a functionally graded material

We consider transient diffusion in a functionally graded material with a diffusion coefficient that has a uniform random distribution with the following functional form

$$k(\mathbf{x},\omega) = k_0(\mathbf{x}) + k_1(\mathbf{x})\xi(\omega), \tag{54}$$

where $\xi(\omega)$ is a uniform random variable between -1 and 1, and the coefficients $k_0(\mathbf{x})$ and $k_1(\mathbf{x})$ are defined as

$$k_0(\mathbf{x}) = 1 + \left(\frac{2 + P\sin(2\pi x/\epsilon_0)}{2 + P\cos(2\pi y/\epsilon_0)} + \frac{2 + \sin(2\pi y/\epsilon_0)}{2 + P\sin(2\pi x/\epsilon_0)}\right)^{-1},$$
$$k_1(\mathbf{x}) = \left(\frac{2 + P\sin(2\pi x/\epsilon_1)}{2 + P\cos(2\pi y/\epsilon_1)} + \frac{2 + \sin(2\pi y/\epsilon_1)}{2 + P\sin(2\pi x/\epsilon_1)}\right)^{-1},$$

where the parameters $\epsilon_0 = 0.08$ and $\epsilon_1 = 0.04$ control the periodicity of $k(\mathbf{x},\omega)$. The parameter $P = 1.8$ controls the ratio of maximum to minimum value of the diffusion coefficient. This specification of the diffusion coefficient can lead to large deviations about the mean solution (of the order of 40%).

Since the diffusion coefficient can be represented using one uniform random variable ξ, the KL dimension of the problem is one. Hence, we use a one-dimensional GPCE in Legendre chaos polynomials [37]. The fully-resolved finite element solution is approximated using the following one-dimensional, fourth-order Legendre chaos expansion (yielding a 5 term expansion)

$$u(\mathbf{x},t,\theta) = u_0 + u_1\zeta_1(\omega) + u_2\zeta_2(\omega) + u_4\zeta_4(\omega) + u_4\zeta_4(\omega),$$

where ($\zeta_1 = \xi$, $\zeta_2 = (3\xi^2 - 1)/2,\ldots$) [25], and the expansion coefficients ($u_0, u_1, u_2,\ldots$) are deterministic functions of $\mathbf{x}$ and t. The computational details for the example are provided in Table 1.

Table 1
Computational parameters used in Example I

Coarse mesh discretization	20×20 and 10×10, respectively
Subgrid mesh discretization	10×10 and 20×20, respectively
GPCE on coarse grid	one-dimensional, third-order Legendre chaos
GPCE on subgrid	one-dimensional, third-order Legendre chaos
Mesh for fully-resolved case	200×200
GPCE for fully-resolved case	one-dimensional, fourth-order Legendre chaos
Coarse time step used	1e − 2 (non-dimensional)
Subgrid time step used	1e − 3 (non-dimensional)
Time step for fully-resolved case	5e − 4 (non-dimensional)
Times for comparison of solutions	0.05 and 0.2
Duration of simulation	0–0.2 (non-dimensional)
Burn-in time for VMS simulation	0.05

As a representative example, we consider the decay of a sine hill with time. This example comprises of an initial sinusoidal temperature distribution that decays with time. It is of interest to study the effect of upscaling error on the solution profile by comparing the VMS solutions with a fully-resolved finite-element solution.

The initial and boundary conditions are deterministic and are chosen as follows:

$$u(\mathbf{x}, 0, \omega) = \sin(\pi x)\sin(\pi y), (x, y) \in [0, 1],$$
$$u|_{x=0} = u|_{x=1} = u|_{y=0} = u|_{y=1} = 0.$$

To assess the accuracy of the upscaling algorithm and to calculate the propagation of upscaling error with time, we performed three simulations: (i) A fully-resolved stochastic FEM computation, (ii) Stochastic VMS computation with dynamic calculation on the subgrid (C2S map and the affine corrections are calculated and stored for each coarse time step), and (iii) Stochastic VMS computation with a quasistatic subgrid assumption (a steady-state solution is obtained for the C2S map and the affine correction at the start of the computation).

Comparison of fully-resolved and stochastic VMS computations: The reconstructed fine-scale solution viz. $(u^{C} + \hat{u}^{F} + u^{F0})$ is obtained for the stochastic VMS computations at times 0.05 and 0.2, respectively. At time 0.05, the time level marking the end of burn-in period (see Section 3.6), the first few coefficients (u_0, u_1 and u_2) in the GPCE expansion of the fully-resolved stochastic FEM solution are shown in Fig. 2A–C, respectively. The same coefficients (u_0, u_1 and u_2) in the reconstructed fine-scale solution obtained using a quasistatic subgrid assumption are shown in Fig. 2D–F. The corresponding plots for a dynamic subgrid assumption are shown in Fig. 2G–I.

The corresponding comparison plots at the final time level 0.2 are shown in Fig. 3A through I. It can be noted that both dynamic and quasistatic subgrid assumptions capture the essential solution characteristics, namely, a decaying sine hill profile. However, in comparison to the dynamic subgrid assumption, the relative magnitude of the GPCE coefficients in the upscaled solution using the quasistatic subgrid assumption are closer to the values of the corresponding GPCE coefficients obtained using a fully-resolved stochastic finite element simulation.

L_2 error between fully-resolved and reconstructed fine-scale solutions: To further check the accuracy of the proposed stochastic VMS method with respect to the coarse and fine-scale discretizations, we perform simulations for two different configurations: (i) A 20×20 coarse-mesh with a 10×10 subgrid mesh in each coarse element, and (ii) A 10×10 coarse-mesh with a 20×20 subgrid mesh in each coarse element. As discussed previously in Section 4.3, the error between the fully-resolved stochastic finite element solution and the fine-scale reconstruction of the VMS solution is characterized by the error in each GPCE coefficient as described by Eqs. (52) and (53). The error terms for a quasistatic subgrid assumption are plotted as a function of time for the case of a 10×10 coarse-mesh with a 20×20 subgrid mesh in Fig. 4A and a 20×20 coarse-mesh with a 10×10 subgrid mesh in Fig. 4B. The corresponding error plots for the dynamic subgrid with a burn-in time of 0.05 are given in Fig. 4C and D, respectively. The various error terms in GPCE coefficients are scaled in order to show them on the same plot.

There are two observations to be made from the error plot:

(1) *The error values for the quasistatic subgrid assumption are consistently lower than those with a dynamic subgrid assumption:* This is attributed to the insufficient accuracy of the boundary conditions and initial conditions provided for the subgrid C2S map and the subgrid affine correction term. It is assumed that at the start of simulation that the subgrid C2S map and the affine correction terms are identically zero in each coarse element. This implies that the boundary conditions for the C2S map are essentially defined at the coarse-scale. Hence, until the subgrid solutions evolve in time and reach an appreciable value, the coarse-scale variational formulation will contain a negligible subgrid contribution. Further, the effect of subgrid contribution of initial conditions on the evolution of affine correction term is not accounted for. Unless, these shortcomings are resolved (as a part of future research), a quasistatic subgrid assumption is a better alternative to the dynamic subgrid assumption.

(2) *The error term E_1 has a non-monotonic behavior:* Initially, the solution is deterministic. As we step in time, the higher-order terms in GPCE of the solution begin to evolve. The maximum rate of evolution is for the first-order term and hence the error increases. However, further ahead in time, the error terms stabilize and show pronounced decaying characteristics.

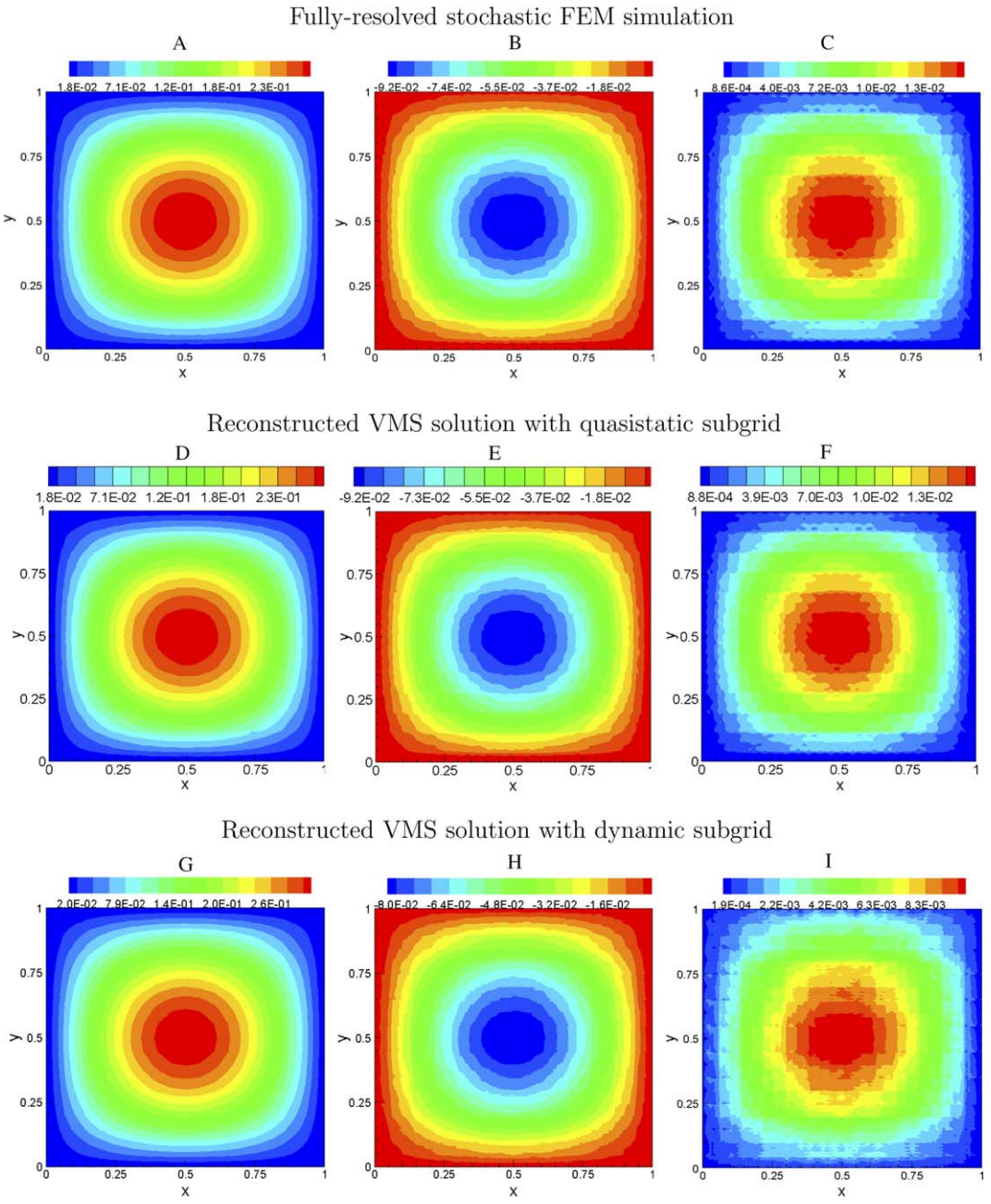

Fig. 2. Example I – decay of a sine hill (*results at time* = 0.05): (A)–(C) Coefficients u_0, u_1 and u_2 obtained from the GPCE of the fully-resolved stochastic finite element solution. (D)–(F) Coefficients u_0, u_1 and u_2 obtained from the GPCE of the fine-scale reconstruction of the VMS solution with a quasistatic subgrid assumption. (G)–(I) Coefficients u_0, u_1 and u_2 obtained from the GPCE of the fine-scale reconstruction of the VMS solution with a dynamic subgrid assumption.

5.2. Example II: transient diffusion in a two-phase microstructure

A gray scale image of a representative two-phase (α and β) microstructure is shown in Fig. 5 [49]. The intensities (I) are scaled to $[0,1]$. Let pure α-phase and pure β-phase be associated with scaled intensities $I = 0$ and $I = 1$, respectively. Any other intensity value between 0 and 1 is associated with a mixture of α and β phases.

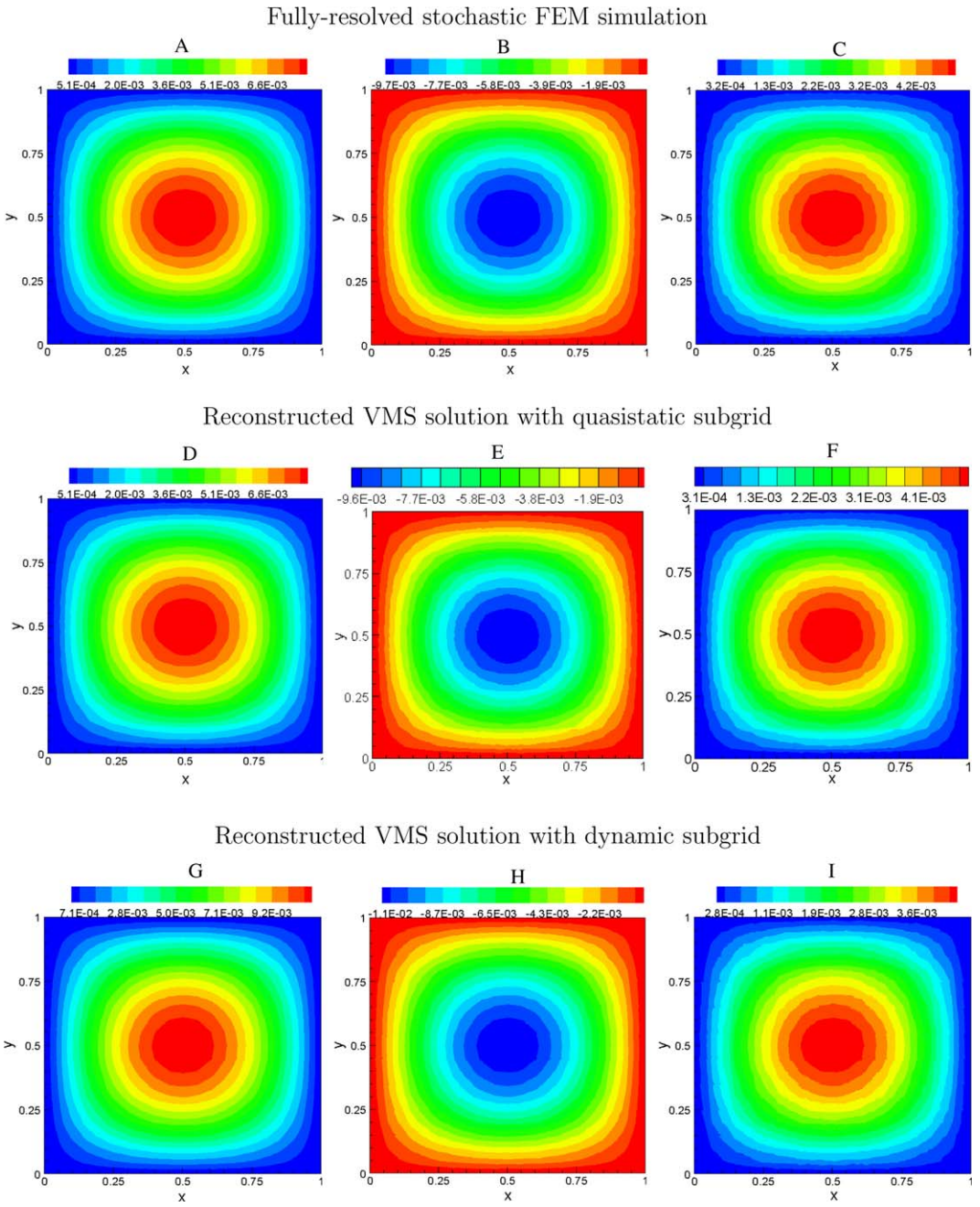

Fig. 3. Example I – decay of a sine hill (*results at time* = 0.2): (A)–(C) Coefficients u_0, u_1 and u_2 obtained from the GPCE of the fully-resolved stochastic finite element solution. (D)–(F) Coefficients u_0, u_1 and u_2 obtained from the GPCE of the fine-scale reconstruction of the VMS solution with a quasistatic subgrid assumption. (G)–(I) Coefficients u_0, u_1 and u_2 obtained from the GPCE of the fine-scale reconstruction of the VMS solution with a dynamic subgrid assumption.

Probability model – We assume that the pure α and pure β-phases have the following uniformly distributed thermal conductivities

$$k_\alpha(\omega) = k_{\alpha 0} + k_{\alpha 1}\xi_1(\omega), \text{ and } k_\beta(\omega) = k_{\beta 0} + k_{\beta 1}\xi_2(\omega), \tag{55}$$

where $\xi_1(\omega)$ and $\xi_2(\omega)$ are two independent uniform random variables defined on the interval $[-1, 1]$. We use the following mixture model for defining the thermal conductivity at a given location on the microstructure:

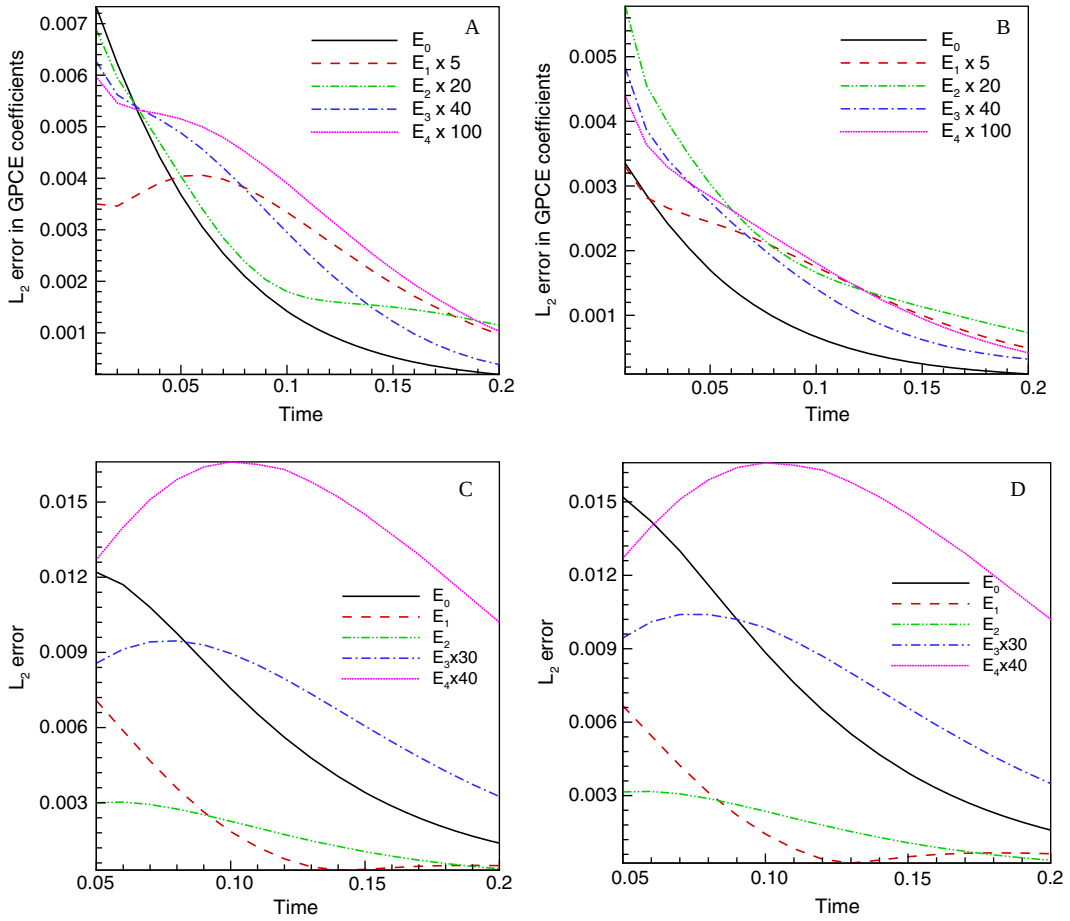

Fig. 4. Example I – decay of a sine hill: Plot of L_2 error in GPCE coefficients vs time: (Quasistatic subgrid case). (A) For a 10×10 coarse-mesh with a 20×20 subgrid mesh. (B) For a 20×20 coarse-mesh with a 10×10 subgrid mesh. (Dynamic subgrid case) (C) For a 10×10 coarse-mesh with a 20×20 subgrid mesh. (D) For a 20×20 coarse-mesh with a 10×10 subgrid mesh.

$$k(\mathbf{x},\omega) = (k_\beta(\omega) - k_\alpha(\omega))I(\mathbf{x}) + k_\alpha(\omega), \tag{56}$$

where $I(\mathbf{x})$ is the scaled intensity at a point $\mathbf{x}$ on the microstructure. Thus, Eq. (56) yields the following two-dimensional random variable model for thermal conductivity:

$$\begin{aligned} k(\mathbf{x},\omega) &= k_0(\mathbf{x}) + k_1(\mathbf{x})\xi_1(\omega) + k_2(\mathbf{x})\xi_2(\omega), \\ k_0(\mathbf{x}) &= (k_{\beta 0} - k_{\alpha 0})I(\mathbf{x}) + k_{\alpha 0}, \\ k_1(\mathbf{x}) &= k_{\alpha 1}(1 - I(\mathbf{x})), \text{ and } k_2(\mathbf{x}) = k_{\beta 1}I(\mathbf{x}). \end{aligned} \tag{57}$$

GPCE model – Since the input distribution is uniform (two-dimensional), a two-dimensional, third-order Legendre chaos expansion (yielding a 10 term expansion) was used for representing the solution. The first few terms in the expansion are shown below:

$$u(\mathbf{x},t,\theta) = u_0 + u_1\xi_1(\omega) + u_2\xi_2(\omega) + u_3(3\xi_1^2(\omega) - 1)/2, + u_4\xi_1(\omega)\xi_2(\omega) + u_5(3\xi_2^2(\omega) - 1)/2 + \cdots, \tag{58}$$

where it is tacitly assumed that the expansion coefficients u_0, u_1 and so forth are deterministic functions of $\mathbf{x}$ and t.

Here, we choose the following initial condition

$$u_0(\mathbf{x},\omega) = 0, \quad \mathbf{x} = (x,y) \in [0,1] \times [0,1], \quad \omega \in \Omega, \tag{59}$$

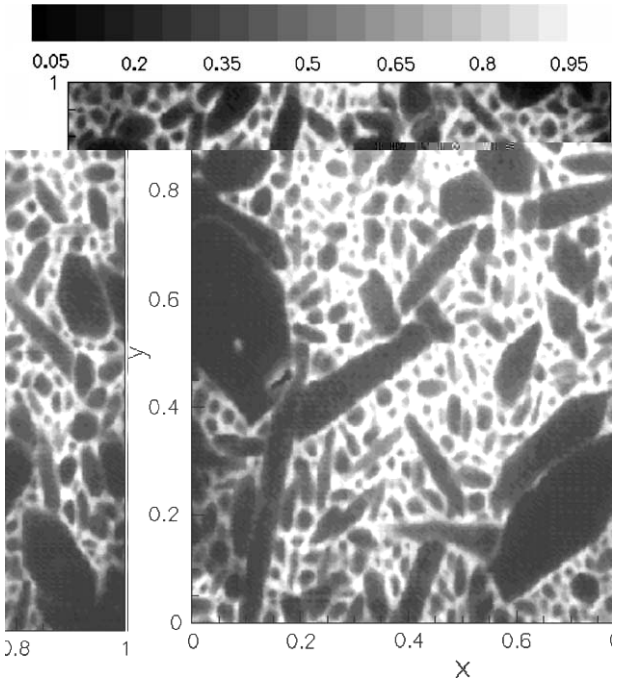

Fig. 5. A gray scale plot of a two-phase (α–β) microstructure. The intensities are scaled to the interval [0, 1] with zero representing the pure α-phase and one representing the pure β-phase.

and the following boundary conditions are imposed

$$k\frac{\partial u}{\partial y} = 0, \quad \text{at } y = 0, 1; \quad u = 0, \text{ at } x = 1; \quad u = 1, \quad \text{at } x = 0. \tag{60}$$

The computational parameters for the example are provided in Table 2.

For the first simulation, we used a 20×20 coarse-mesh with an underlying 10×10 subgrid mesh for each coarse element. The coefficients (u_0, u_1 and u_2) in the GPCE expansion of the solution at time 0.05 as obtained in the fully-resolved stochastic finite element simulation are shown in Figs. 6A–C, respectively. The same coefficients obtained by reconstruction of the fine-scale solution (from the coarse-scale solution obtained using the stochastic VMS method) using the quasistatic assumption are shown in Figs. 6D–F, respectively. The computed upscaled coarse solution (i.e. the coarse-scale solution obtained from the VMS formulation after the application of C2S map and the affine correction term) is shown in Figs. 6G–I, respectively. In order to compare the upscaled coarse solution for various coarse discretizations, we recomputed the coarse solution for a

Table 2
Computational parameters used in Example II

Coarse mesh discretization	20×20 and 10×10, respectively
Subgrid mesh discretization	10×10 and 20×20, respectively
GPCE on coarse grid	two-dimensional, third-order Legendre chaos
GPCE on subgrid	two-dimensional, third-order Legendre chaos
Mesh for fully-resolved case	200×200
GPCE for fully-resolved case	two-dimensional, fourth-order Legendre chaos
Coarse time step used	1e − 3 (non-dimensional)
Subgrid time step used	5e − 4 (non-dimensional)
Time step for fully-resolved case	1e − 3 (non-dimensional)
Times for comparison of solutions	0.05 and 0.2
Duration of simulation	0–0.2 (non-dimensional)
Burn-in time for VMS simulation	0.05

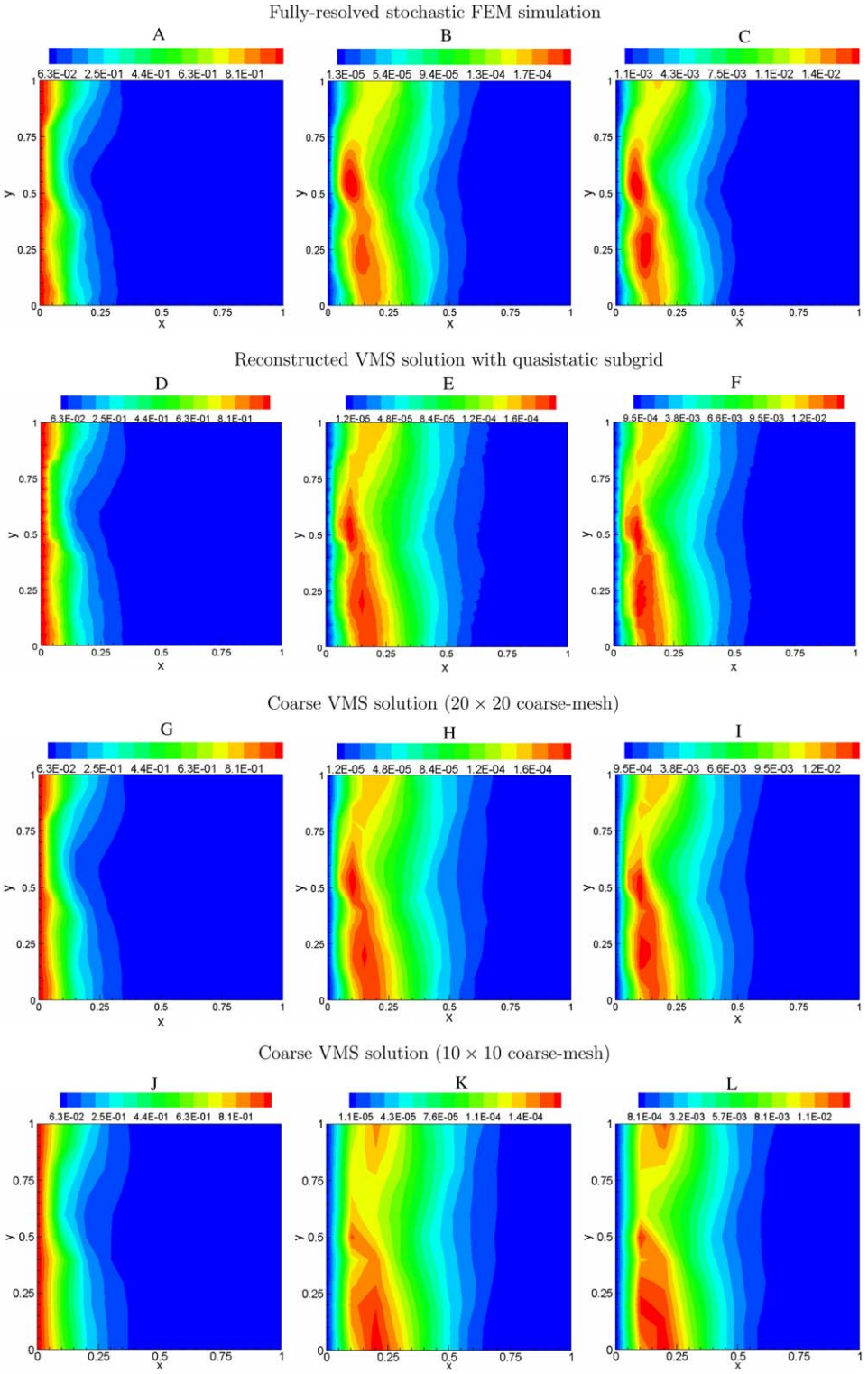

Fig. 6. Example II – diffusion in a microstructure (results at time 0.05): Coefficients u_0, u_1 and u_2 in the GPCE of the solution for the following: (A)–(C) Fully-resolved stochastic finite element solution. (D)–(F) Fine-scale reconstruction of the VMS solution with a quasistatic subgrid assumption (20×20 coarse-mesh, 10×10 subgrid mesh). (G)–(I) Coarse-scale solution (20×20 coarse-mesh). (J)–(L) Coarse-scale solution (10×10 coarse-mesh).

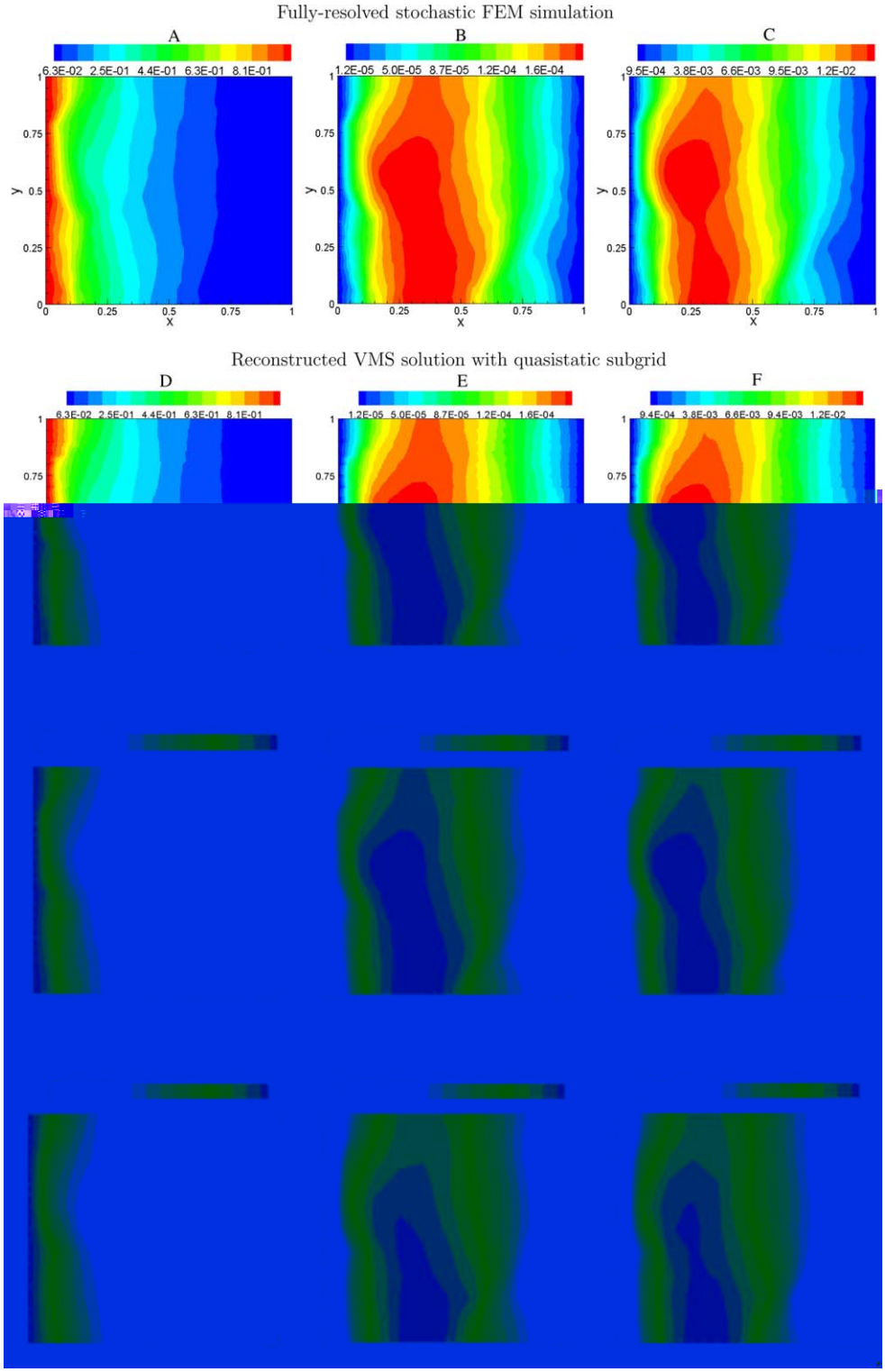

Fig. 7. Example II – diffusion in a microstructure (results at time 0.2): Coefficients u_0, u_1 and u_2 in the GPCE of the solution for the following: (A)–(C) Fully-resolved stochastic finite element solution. (D)–(F) Fine-scale reconstruction of the VMS solution with a quasistatic subgrid assumption (20×20 coarse-mesh, 10×10 subgrid mesh). (G)–(I) Coarse-scale solution (20×20 coarse-mesh). (J)–(L) Coarse-scale solution (10×10 coarse-mesh).

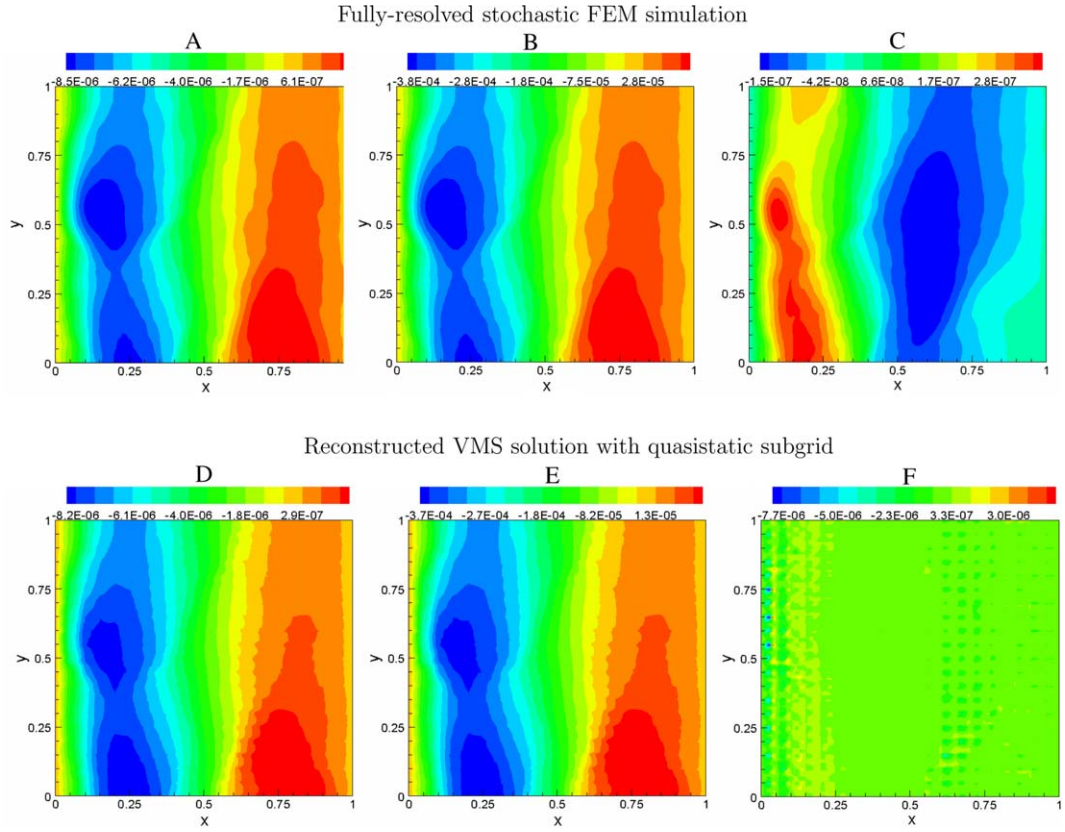

Fig. 8. Example II – (A)–(C) Fully-resolved stochastic FEM simulation: coefficients u_3, u_4 and u_5 in the GPCE expansion of the solution. (D)–(F) Fine-scale reconstruction of the stochastic solution using a quasistatic subgrid assumption in the VMS simulation: Coefficients u_3, u_4 and u_5 in the GPCE expansion of the solution obtained at time 0.2 (non-dimensional).

10×10 coarse-mesh with an underlying 20×20 subgrid mesh. The results are shown in Figs. 6J–L. It can be observed that the coarse solution is more diffused. This indicates that the coarse-mesh requires an optimum discretization level for maintaining solution accuracy. More research is required in this regard. Finally, the corresponding coefficients at time 0.2 are shown in Figs. 7A–I.

Plots showing comparison of higher-order GPCE coefficients in the fully-resolved stochastic finite element solution and the reconstructed fine-scale VMS solution are shown in Figs. 8A–F. It can be noticed that the GPCE coefficient u_6 in the reconstructed fine-scale VMS solution exhibits oscillations and is consequentially incorrect. This could be attributed to the L_2 nature of the upscaling method. It can be noticed that the scale of the u_5 term (order of 10^{-7}) is negligible in comparison with the mean solution u_0 (order of 10^{-1}) or the first-order GPCE coefficients u_1 and u_2 (order of 10^{-4} and 10^{-3}, respectively). As a result, the contribution of error in u_5 to the L_2 error in the upscaled solution is negligible. To improve the solution quality for such small GPCE terms, we would require a weighted upscaling technique. This would be a part of our future research.

6. Conclusions

A stochastic variational multiscale formulation was proposed for addressing transient diffusion problems in random heterogeneous media with the diffusion coefficient having multiple length scales. The main idea was to capture the diffusion dynamics on a highly coarse-mesh by including localized solutions to subgrid problems. For this, the variational formulation for the governing diffusion equation was decomposed into a coarse-scale and a subgrid scale part. The subgrid part was then localized in each coarse element sub-domain and a class of subgrid models was derived for one-step generalized trapezoidal time integration rules. The generalized

polynomial chaos method was used for representation and solution of all the resulting stochastic PDEs (the coarse variational formulations and the localized subgrid problems).

The algorithms presented do not yet consider the effect of resonance error in linking the coarse and fine/subgrid scales in any rigorous detail. Further requirements include developing a mathematically consistent adaptive algorithm for selecting the number of element sub-divisions in each fine-scale mesh, adaptive generation of subgrid bases and other. Also to be considered in future works are the issues of improving fine-scale reconstruction of the stochastic solution using a weighted subgrid model. These issues are currently being addressed for extending the current VMS algorithms to the solution of advection-dominant problems in heterogeneous media.

Acknowledgements

The work presented here was funded in part by the Computational Mathematics program of the Air Force Office of Scientific Research (Grant F49620-00-1-0373). The computing for this project was supported by the Cornell Theory Center, which receives funding from Cornell University, New York State, federal agencies, and corporate partners.

References

[1] T.Y. Hou, X.H. Wu, A multiscale finite element method for elliptic problems in composite materials and porous media, J. Comput. Phys. 134 (1997) 169–189.
[2] G. Milton, Theory of Composites, Cambridge University Press, Cambridge, UK, 2002.
[3] T. Arbogast, Analysis of a two-scale, locally conservative subgrid upscaling for elliptic problems, SIAM J. Numer. Anal. 42 (2004) 576–598.
[4] T. Arbogast, S.L. Bryant, A two-scale numerical subgrid technique for waterflood simulations, SPE J. (2002) 446–457.
[5] P. Renard, G. de Marsily, Calculating equivalent permeability: a review, Adv. Water Res. 20 (1997) 253–278.
[6] T. Arbogast, S.E. Minkoff, P.T. Keenan, An operator-based approach to upscaling the pressure equation, Computational Methods in Water Resources XIIComputational Methods in Contamination and Remediation of Water Resources, Vol. 1, Computational Mechanics Publications, Southampton, UK, 1998.
[7] T. Arbogast, Implementation of a locally conservative numerical subgrid upscaling scheme for two-phase darcy flow, Comput. Geosci. 6 (2002) 453–480.
[8] T. Arbogast, Numerical subgrid upscaling of two-phase flow in porous media, Lecture Notes in Physics, vol. 552, Springer, Berlin, 2000.
[9] W.E.B. Engquist, The heterogeneous multi-scale methods, Comm. Math. Sci. 1 (1) (2003) 87–133.
[10] W.E.P.B. Ming, P.W. Zhang, Analysis of the heterogeneous multiscale method for elliptic homogenization problems, preprint, 2003.
[11] T.Y. Hou, X.H. Wu, Z.Q. Cai, Convergence of a multiscale finite element method for elliptic problems with rapidly oscillating coefficients, Math. Comput. 68 (1999) 913–943.
[12] P. Park, T.Y. Hou, Multiscale numerical methods for singularly-perturbed convection diffusion equations, Intl. J. Comput. Meth. 1 (1) (2004) 17–65.
[13] Y. Efendiev, V. Ginting, T.Y. Hou, R. Ewing, Accurate multiscale finite element methods for two-phase flow simulations, J. Comput. Phys, submitted.
[14] I. Babuska, U. Banerjee, J. Osborn, Generalized finite element methods: main ideas, results and perspective, Int. J. Comput. Meth. 1 (2004) 67–103.
[15] L.P. Franca, A.L. Madureira, F. Valentin, Towards multiscale functions: enriching finite element spaces with local but not bubble-like functions, Comp. Meth. Appl. Mech. Eng. 194 (27–29) (2005) 3006–3021.
[16] H.J. Pradlwarter, G.I. Schueller, A state-of-the-art report on computational stochastic mechanics, Probabil. Eng. Mech. 12 (4) (1997) 197–322.
[17] T. Hisada, S. Nakagiri, Role of stochastic finite element methods in structural safety and reliability, in: Proceedings of 4th International Conference on Structural Safety and Reliability, Kobe, Japan, 1985, pp. 385–394.
[18] M. Shinozuka, G. Deodatis, Response variability of stochastic finite element systems, J. Eng. Mech. (ASCE) 114 (3) (1988) 499–519.
[19] D. Xiu, G.E. Karniadakis, Modeling uncertainty in flow simulations via generalized polynomial chaos, J. Comput. Phys. 187 (2003) 137–167.
[20] M. Loève, Probability Theory, fourth ed., Springer-Verlag, Berlin, 1977.
[21] R.H. Cameron, W.T. Martin, The orthogonal development of nonlinear functionals in series of fourier hermite functionals, Ann. Math. 48 (1947) 385–392.
[22] R. Ghanem, P. Spanos, Stochastic Finite Elements: A Spectral Approach, Springer-Verlag, Berlin, 1991.
[23] O.P. Le Maître, O.M. Kino, H.N. Najm, R. Ghanem, A stochastic projection method for fluid flow I. Basic formulation, J. Comput. Phys. 173 (2001) 481–511.

[24] O.P. Le Maître, M. Reagan, R. Ghanem, O.M. Kino, A stochastic projection method for fluid flow II. Random process, J. Comput. Phys. 181 (2002) 9–44.
[25] D. Xiu, D. Lucor, C.H. Su, G.E. Karniadakis, Stochastic modeling of flow-structure interactions using generalized polynomial chaos, J. Fluids. Eng. 125 (2001) 51–59.
[26] B.J. Debusschere, H.N. Najm, P.P. Pébay, O.M. Knio, R.G. Ghanem, O.P. Le Maître, Numerical challenges in the use of polynomial chaos representations for stochastic processes, SIAM J. Sci. Comput. 26 (2) (2004) 698–719.
[27] Y. Efendiev, A. Pankov, Numerical homogenization of nonlinear random parabolic operators, SIAM MMS 2 (2) (2004) 237–268.
[28] Y. Efendiev, A. Pankov, Numerical homogenization and correctors for random nonlinear elliptic equations, SIAM J. Appl. Math. 65 (1) (2004) 43–68.
[29] T.J.R. Hughes, Multiscale phenomena: Green's functions, the dirichlet-to-neumann formulation, subgrid scale models, bubbles and the origin of stabilized methods, Comp. Meth. Appl. Mech. Eng. 127 (1995) 387–401.
[30] T.J.R. Hughes, G.R. Feijóo, L. Mazzei, J.B. Quincy, The variational multiscale method – a paradigm for computational mechanics, Comp. Meth. Appl. Mech. Engrg. 166 (1998) 3–24.
[31] R. Ghanem, Ingredients for a general purpose stochastic finite element formulation, Comp. Meth. Appl. Mech. Eng. 168 (1999) 19–34.
[32] B. Velamur Asokan, N. Zabaras, Variational multiscale stabilized fem formulations for transport equations: stochastic advection-diffusion and incompressible stochastic navier-stokes equations, J. Computat. Phys. 202 (2004) 94–133.
[33] B. Velamur Asokan, N. Zabaras, Using stochastic analysis to capture unstable equilibrium in natural convection, J. Computat. Phys. 208 (2005) 134–153.
[34] O.P. Le Maître, O.M. Kino, R. Ghanem, H.N. Najm, A stochastic projection method for microchannel flow, Mod. Sim. Microsystems 181 (2002) 9–44.
[35] N. Wiener, The homogeneous chaos, Am. J. Math. 60 (1930) 897–936.
[36] M. Jardak, C.-H. Su, G.E. Karniadakis, Spectral polynomial chaos solutions of the stochastic advection equation, J. Sci. Comput. 17 (2002) 319–338.
[37] X. Wan, G.E. Karniadakis, An adaptive multi-element generalized polynomial chaos method for stochastic differential equations, Tech. rep., BrownSC-2005-07, Brown University, 2005.
[38] S.I. Resnick, A Probability Path, Birkhäuser, Boston, USA, 2001.
[39] D. Xiu, G.E. Karniadakis, The Wiener–Askey polynomial chaos for stochastic differential equations, SIAM J. Sci. Comput. 24 (2) (2002) 619–644.
[40] R.V. Field Jr., M. Grigoriu, On the accuracy of the polynomial chaos expansion, Probabil. Eng. Mech. 19 (2004) 65–80.
[41] D.G. Luenberger, Optimization by Vector Space Methods, John Wiley & Sons Inc., New York, NY, USA, 1997.
[42] G. Sangalli, Capturing small scales in elliptic problems using a residual-free bubbles finite element method, SIAM MMS 1 (3) (2003) 485–503.
[43] J.E. Aarnes, V. Kippe, K.A. Lie, Mixed multiscale finite elements and streamline methods for reservoir simulation of large geomodels, Adv. Water Res. 28 (3) (2005) 257–271.
[44] D. Xiu, I.G. Kevrekidis, Equation-free, multiscale computation for unsteady random diffusion, SIAM MMS 4 (3) (2005) 915–935.
[45] C.I. Siettos, A. Armaou, A.G. Makeev, I.G. Kevrekidis, Microscopic/stochastic timesteppers and coarse control: a kinetic monte carlo example, AIChE J. 49 (7) (2003) 1922–1926.
[46] W. Gear, I.G. Kevrekidis, C. Theodoropoulos, "Coarse" integration/bifurcation analysis via microscopic simulators: micro-Galerkin methods, Comp. Chem. Eng. 26 (2002) 941–963.
[47] B. Velamur Asokan, N. Zabaras, Stochastic inverse heat conduction using a spectral approach, Intl. J. Num. Meth. Eng. 60 (9) (2004) 1569–1593.
[48] D. Xiu, G.E. Karniadakis, A new stochastic approach to transient heat conduction modeling with uncertainty, Int. J. Heat Mass Transf. 46 (24) (2003) 4681–4693.
[49] C. Carter, Available from: <http://pruffle.mit.edu/ccarter/oof/gallery/>.